# Flight Study of Induced Turbofan Inlet Acoustic Radiation with Theoretical Comparisons

J. S. Preisser* and R. J. Silcox*
*NASA Langley Research Center, Hampton, Virginia*
and
W. Eversman† and A. V. Parrett‡
*University of Missouri-Rolla, Rolla, Missouri*

**This paper presents a study of acoustic tone radiation patterns from a small turbofan engine in flight and compares results with similar static test stand data and a recently developed radiation theory. An interaction tone was induced for test and evaluation purposes by placing a circumferential array of inlet rods just upstream of the fan blades. Overhead and sideline flight directivity patterns showed cut-on of a dominant single-mode tone occurred at the predicted fan speed, and there was an absence of any other significant circumferential or radial modes. In general, good agreement was found between measured flight and static data, with small differences being attributed to inlet geometry and/or forward speed effects. Good agreement was also obtained between flight data and theory for directivity pattern shape, however, the theory consistently predicted higher values for peak radiation angle over a wide range of frequency.**

## Nomenclature

$a$ = radius of inlet at throat, = 9.95 in.
$B$ = number of fan blades
$c$ = speed of sound at inlet throat, in./s
$f$ = frequency, Hz
$K_{m,\mu}$ = mode eigenvalue
$k$ = free-space wave number, $=2\pi f/c$, in.$^{-1}$
$M_{th}$ = Mach number at inlet throat
$M_{tip}$ = Mach number of fan tip
$M_\infty$ = Mach number of aircraft or freestream Mach number
$N_f$ = fan speed, rpm
$(m,\mu)$ = (circumferential, radial) duct mode numbers
$R$ = radial distance to far field in spherical coordinates, in.
$r$ = cylindrical radial coordinate, in.
$x$ = cylindrical axial coordinate, in.
$\theta$ = directivity angle measured from inlet axis in spherical coordinates, deg
$\xi$ = cutoff ratio, $=BM_{tip}/K_{m,\mu}\sqrt{1-M_{th}^2}$
$\phi$ = sideline or polar angle, deg (see Fig. 5)

## Introduction

CONTINUING progress is being made in reducing inlet noise produced by turbofan aircraft. Current emphasis is on achieving the required suppression while imposing minimal aerodynamic and fuel consumption penalties. This requirement dictates a better understanding of acoustic liners and the effects of inlet geometry and flow on acoustic radiation. In addition, the desire to base noise certification of aircraft on flight tests of one airplane while subsequent derivatives are certified through analysis and/or static engine noise measurements makes it imperative that inlet radiation, both static and flight, be clearly understood.

Inlet radiation has been studied extensively in the laboratory by analytical modeling, and during engine static tests. For example, laboratory experiments[1,2] have demonstrated the importance of inlet geometry on radiation close to cut-on of an acoustic spinning mode, while in-duct flow was found to have little effect on radiation directivity regardless of inlet geometry. Efforts in modeling the radiation from inlets[3,4] have proven quite successful in predicting the no-flow and in-duct-flow laboratory data. A recent report[5] shows good agreement between theory and static engine test stand data and predicts what the radiation directivity would be from the same engine in flight. Unfortunately, the lack of flight radiation data from inlets with known modal structure makes it difficult to assess the accuracy of such predictions for the flight environment.

A recently concluded NASA inter-Center program designed to evaluate ground test techniques for flight simulation compared the far field acoustic spectra and radiation patterns for ground, wind tunnel, and flight conditions.[6] This datum was for a typical small turbofan engine, namely the JT15D. Fan blade-mounted transducers were used to infer the existence of several duct spinning modes although it was not known if higher order radials or other unknown circumferential modes contributed much energy to the far-field radiation. The present paper is concerned with flight data for a modified JT15D engine. In particular, a circumferential array of small-diameter rods protruded from the inlet wall into the flow just upstream of the fan blades. The intent was that the resulting interaction between the rod wakes and fan blades would produce a single intense known acoustic spinning mode at the blade passage frequency (BPF). The approach of placing rods in front of the fan blades to generate a pure tone for test and evaluation purposes was employed successfully in the ground test program of Ref. 7, which used a similar JT15D engine but with a different inlet geometry. Using the rod-fan interaction as a demonstrable single-mode tone source, this paper correlates the flight-test radiation characteristics with the static test results[7] and a recently developed radiation theory.[4] To the knowledge of the

Presented as Paper 84-0499 at the AIAA 22nd Aerospace Sciences Meeting, Reno, Nev., Jan. 9-12, 1984; received March 10, 1984; revision received Aug. 6, 1984. This paper is declared a work of the U.S. Government and therefore is in the public domain.

*Aerospace Engineer, Noise Propagation and Suppression Branch, Acoustics and Noise Reduction Division. Member AIAA.
†Professor. Associate Fellow AIAA.
‡Graduate Student.

authors, these results are the only available data for a simple, clearly identifiable noise source radiating from a turbofan inlet in flight.

## Test Description

### Testbed Aircraft and Modified Engine

A photograph of an OV-1B test aircraft is presented in Fig. 1. The JT15D was installed under the right wing outboard of the right turboprop engine. The flight tests were performed with the right turboprop shut down and feathered to minimize in-flow distortion to the JT15D which could alter the inlet noise radiation of interest. Development of the testbed aircraft and engine/inlet performance are fully described in Ref. 8.

The JT15D is a small (2200-lb thrust) turbofan engine with 28 fan blades. It has a bypass stator and a modified core stator such that both rotor-stator interaction mechanisms are acoustically cut-off over the engine operating range. The rods used to produce the interaction tone were 3/16-in.-diam stainless steel and protruded 2.5 in. from the wall into the duct. They were mounted about 3 in. in front of the leading edge of the fan blades and were equally spaced circumferentially around the interior duct wall. There were 41 rods in all. A photograph viewing into the JT15D inlet with rods in place is presented in Fig. 2. The inlet geometry is shown schematically in Fig. 3. The inlet duct was nearly cylindrical varying from 19.9 in. in diameter at the throat to 21.0 in. at the fan. The inlet throat occurred several inches aft of the highlight between axial stations of 0 and $-2.65$. A full geometric description is given in the Appendix.

### Fan Noise Characteristics

According to the Tyler-Sofrin theory[9] the blade passage frequency tone noise arising when rotor wakes interact with stator vanes or when rod wakes interact with a rotor can be described in terms of spinning acoustic modes. A specific mode in cylindrical coordinates can be identified by its circumferential $m$ and radial $\mu$ order usually written as $(m,\mu)$ mode [where (0,0) is the plane-wave mode].

For the present test, the 41 rod array interacting with the 28 fan blades should produce a mode of circumferential order 13. Many radial mode orders are possible. Modal propagation to the far field is determined by cutoff ratio and, as shown in Ref. 9, is a function of rotor tip and duct flow Mach numbers, as well as the particular duct eigenvalue. Figure 4 presents cutoff/propagate ranges for several modes expected to be present in this engine configuration. The lowest order radial mode (13,0) begins to propagate at an engine fan speed of about 6400 rpm (near engine idle conditions). This corresponds to a $ka$ value of about 14. Higher radial order modes begin to propagate at higher fan speeds.

As discussed in Ref. 6, the JT15D turbofan (with modified core stator) is believed to have BPF tone contributions mainly from rotor-strut potential field and rotor 1/rev interactions and from the rotor alone. Based on Tyler-Sofrin theory, these interactions result in $m=22$, 27, and 28 spinning modes which cut-on at fan speeds of 10,650, 12,750, and 13,200 rpm, respectively. Thus, it can be seen from Fig. 4 that, with the rods installed, the lowest three radial orders of $m=13$ can propagate (at the lower fan speeds) before the natural (without rods) engine modes are cut-on.

### Data Acquisition and Reduction

The flight tests made extensive use of several data measuring systems. Engine performance and aircraft state parameters were recorded by tape recorders on the aircraft and post-flight processed. Table 1 presents several pertinent parameters either measured or calculated from the measured data for the various test conditions. The far-field acoustic data were recorded by a linear array of eight ½-in. condenser-type microphones mounted on 30-ft poles situated on a

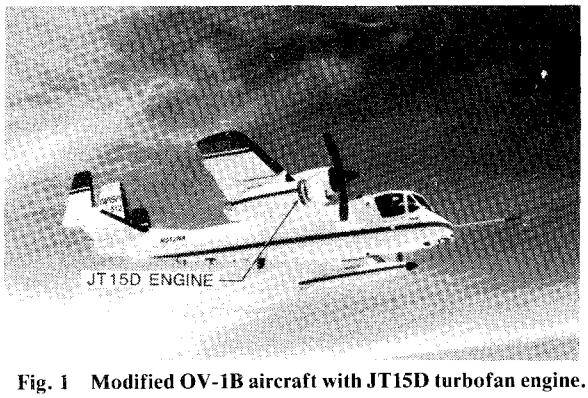


Fig. 1 Modified OV-1B aircraft with JT15D turbofan engine.

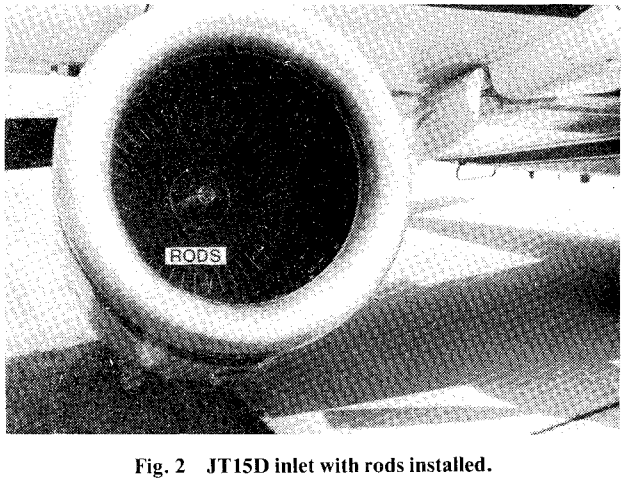


Fig. 2 JT15D inlet with rods installed.

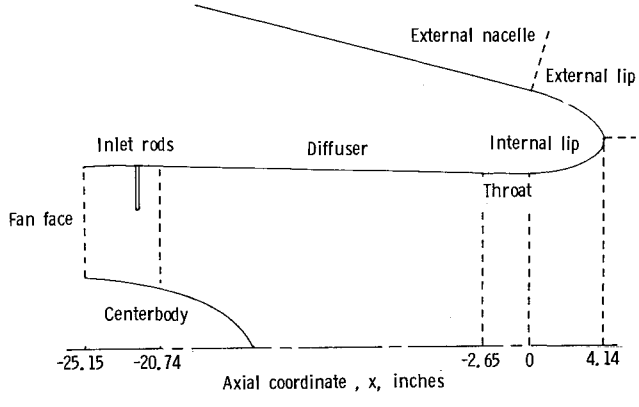


Fig. 3 Schematic of JT15D inlet.

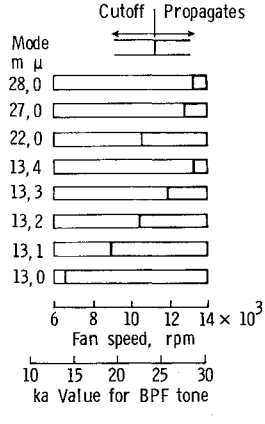


Fig. 4 Mode cut-off ranges of engines with rods.

**Table 1 Flight test parameters**

| $N_1$, rpm | $f$, kHz | $ka$ | $M_\infty$ | $M_{th}$ | $M_{tip}$ | $\xi(13,0)$ | $\xi(13,1)$ | $\xi(13,2)$ |
|---|---|---|---|---|---|---|---|---|
| 11,940 | 5.65 | 26.3 | 0.200 | 0.328 | 0.979 | 1.86 | 1.40 | 1.17 |
| 10,760 | 5.09 | 23.6 | 0.192 | 0.289 | 0.883 | 1.65 | 1.24 | 1.03 |
| 10,460 | 4.94 | 22.9 | 0.192 | 0.280 | 0.858 | 1.60 | 1.20 | 1.00 |
| 9,560 | 4.52 | 20.9 | 0.198 | 0.254 | 0.784 | 1.45 | 1.09 | 0.91 |
| 9,220 | 4.36 | 20.2 | 0.200 | 0.238 | 0.756 | 1.39 | 1.05 | 0.87 |
| 8,610 | 4.07 | 18.8 | 0.203 | 0.227 | 0.706 | 1.29 | 0.97 | 0.81 |
| 8,010 | 3.79 | 17.5 | 0.204 | 0.211 | 0.657 | 1.20 | 0.90 | 0.75 |
| 6,780 | 3.20 | 14.8 | 0.200 | 0.178 | 0.556 | 1.01 | 0.76 | 0.63 |
| 6,210 | 2.94 | 13.6 | 0.199 | 0.166 | 0.510 | 0.92 | 0.69 | 0.58 |

runway at the NASA Wallops Flight Facility. Aircraft flyovers were at a nominal altitude of 300 ft and an airspeed of 220 ft/s. Part of the flyovers were directly over the microphone array; others were off to the left of the array to present a sideline radiation pattern. Figure 5 defines the inlet directivity and sideline angles.

Utilizing laser-radar tracking and weather profile data, the acoustic data were narrowband analyzed (100 Hz), ensemble averaged, and adjusted to a wind tunnel coordinate system under lossless atmospheric conditions at a constant radius of 100 ft (see Ref. 6 for a more complete description). The ensemble averaging over the microphone array provided highly accurate sound pressure levels (SPL) without loss of angular resolution of the inlet emission angle. The adjustment procedure included the following considerations: acoustic retarded time, instrumentation corrections, inverse square law, atmospheric attenuation, ground impedance, and Doppler frequency shift. Such a normalization procedure allowed data sets recorded on different days under varying conditions to be compared directly.

No adjustment was made for convective amplification, since this effect is inherent in the forward speed calculation of Ref. 4, against which the flight data will be compared. The static data of Ref. 7 were analyzed in one-third octave bands and adjusted to a free-field condition at 100-ft radius with atmospheric attenuation removed. In addition to the bandwidth difference, the static test configuration employed an inlet control device and a different inlet lip (more closely representing a bellmouth) than the flight configuration. Implications of the static/flight geometry and data reduction differences will be discussed in a later section.

## Acoustic Radiation Theory

The details of the finite element/wave envelope analysis are given in Ref. 4. The actual flight inlet geometry, as described in the Appendix, was used in the modeling. Analyses were performed with flow in the inlet duct and both with and without external flow to simulate the flight and static cases, respectively. A conventional Galerkin/weighted residual finite element scheme is used in the acoustic near field of the inlet lip to describe the rapid variations likely to occur in this region. The wave envelope formulation of the finite element scheme is used far away from the inlet and incorporates the reciprocal decay and wavelike variation of a locally outward traveling wave into the basis functions. In contrast to the conventional elements used in the near field where each wavelength is modeled over several elements, larger elements that may extend over many wavelengths are chosen in the far field. These elements of differing characteristics are then integrated into an overall matrix equation to be solved simultaneously for the complete solution. In this way, the number of elements or degrees of freedom required for a useful solution in this computationally large domain is kept from becoming prohibitively large in terms of computer resources.

Figure 6 shows a typical radiation contour map illustrating these concepts in terms of contours of constant sound

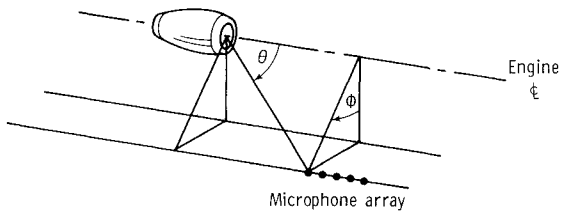


**Fig. 5 Inlet directivity $\theta$ and sideline angle $\phi$.**

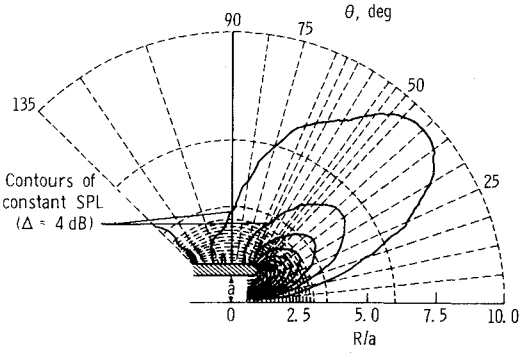


**Fig. 6 Illustrative computational contour map; $ka=3.7$, $m=2$.**

pressure plotted on a background of the finite element/wave envelope mesh for a (2,0) mode at $ka=3.7$. (These particular mode number and $ka$ values are not representative of the present test, but show more clearly the various contours for illustrative purposes.) The contours are in 4-dB increments. The outer region in which the wave envelope scheme is applied contains five layers of elements and extends from about $R/a=2.5$ to 10. The inner region adjacent to the inlet contour represented by the dotted area reflects the much finer mesh needed to represent the rapid variation in acoustic quantities occurring in this region.

## Results and Discussion

### Effects of Inlet Rods

Far-field narrowband (100-Hz bandwidth) acoustic spectra at an inlet radiation angle of 60 deg are presented in Fig. 7 at two slightly different fan speeds, which correspond to $ka$ values of 14.8 and 13.6 for the BPF tone. The calculated cut-on values for the (13,0) mode for these $ka$ values are 1.01 and 0.92, respectively. In accordance with the anticipated change in the far field, the BPF tone level shows a nearly 20-dB increase when cut-on occurs. This increase gives strong evidence for the existence of a very dominant (13,0) mode. One additional observation to be made from Fig. 7 is that before cut-on there is a significant amount of energy at twice the blade passage frequency (2 BPF). Apparently, the rod wakes interacting with the blades excite various propagating modes at

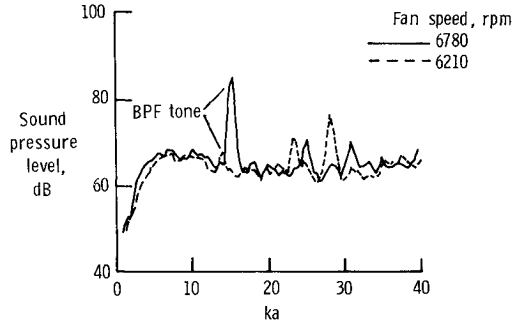


**Fig. 7 Spectra comparison at $\theta = 60$ deg and $\phi = 0$ deg before and after cut-on of (13,0) mode.**

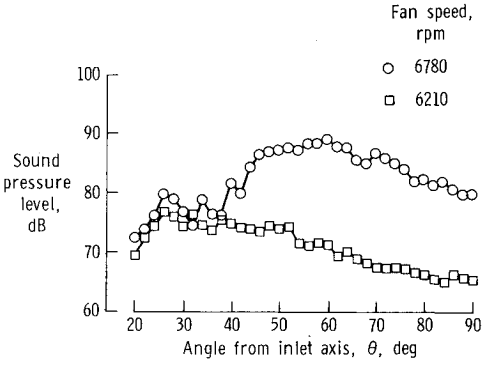


**Fig. 8 Directivity comparisons of BPF tone before and after cut-on of (13,0) mode; $\phi = 0$ deg.**

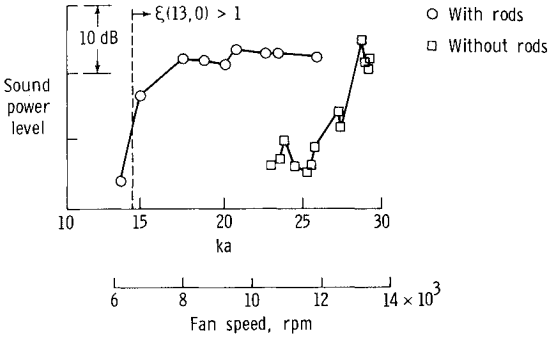


**Fig. 9 Relative BPF tone sound power comparison.**

this higher frequency. Once cut-on occurs, the blade passage frequency becomes the dominant tone.

Directivity patterns of the BPF tone are presented in Fig. 8 for the same two cases as in the previous figure. Prior to cut-on, the peak sound pressure level occurs at about $\theta = 30$ deg. Once the calculated cut-off point is exceeded, a broad increase in level is seen for all angles aft of 40 deg. This radiation toward the sideline is indicative of a mode just after cut-on.

Figure 9 shows inlet radiated acoustic power obtained by integrating the BPF tone level over the forward hemisphere (assuming symmetry in the polar angle which will be shown later). Relative power levels as a function of the *ka* value for the BPF tone are compared for configurations with and without inlet rods. There was no measurable tone in the narrowband (100-Hz) flight data below $ka = 23$ for the no-rod case. Above this value, the tone level increased as rotor-potential field, rotor 1/rev distortion, and rotor-alone noise source mechanisms successively cut-on. In contrast, a tone was always present for the case with rods. The jump in level just before $ka = 15$ is associated with cut-on of the (13,0)

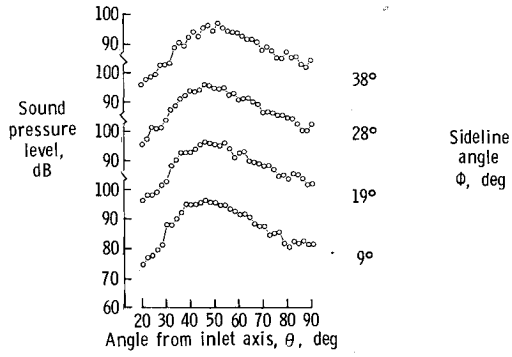


**Fig. 10 Sideline directivity patterns of BPF tone at $ka = 14.8$.**

mode in agreement with the result from the previous figures. No significant increases in level are seen at those *ka* values where the higher order radial modes can propagate. In addition, it appears that the natural JT15D fan noise sources have little effect on the BPF tone level over the range where the rod data were taken. This is to be expected since the rods produced such a dominant tone.

### Sideline Directivity

Several flight tests were conducted off to the side of the microphone array to produce sideline directivity patterns. Results of four such flights are presented in Fig. 10. The sideline or polar angle is measured from the vertical plane passing through the engine centerline, see Fig. 5. The data are for sideline angles of 9, 19, 28, and 38 deg at a *ka* value of 14.8. Only the (13,0) mode would be cut-on here. The directivities have about the same level and shape. Recall that in this paper the flight data have been adjusted to a wind tunnel coordinate system at a constant radius with atmospheric absorption removed. Hence the agreement in the adjusted data imply that the radiated BPF sound pressure level is symmetric with respect to the engine centerline. The absence of asymmetry arising from interference effects among a plurality of spinning modes implies that a single dominant mode is present and, in addition, engine/aircraft installation effects are insignificant.

Sideline directivity patterns for similar polar angles, but at a *ka* value of 22.9, are presented in Fig. 11. At this value, as shown in Fig. 4 and Table 1, the (13,0), (13,1), and (13,2) modes can propagate. Again, the symmetry with respect to sideline angle implies the absence of any contaminating spinning modes. In addition, if all three modes were present with significant energy in each mode, one would expect several peaks in the far-field directivity. The (13,2) mode being just cut-on should exhibit high levels at angles greater than 45 deg. Overall, the migration of a single radiation lobe toward the duct axis, as *ka* increases, is strong evidence of a single-mode source structure.

Figure 12 is presented to demonstrate a physical argument for the dominance of a single mode. The radial dependence of the solution (Bessel functions of the first and second kind) to the wave equation in cylindrical coordinates in terms of acoustic pressure is plotted as a function of radial distance between the centerbody and the inlet wall. At the top of the figure is a sketch showing the position of a typical rod relative to the leading edge of the fan plane. The rod sheds a wake that is more or less in phase over its length. This wake is the exciting force for the pressure field which then couples into the duct modes. Only the (13,0) mode has a radial pressure dependence that does not suffer a phase reversal over the range where the rods are present. Thus, the (13,0) mode presents the best match with the exciting force and is apt to be excited most strongly regardless of frequency.

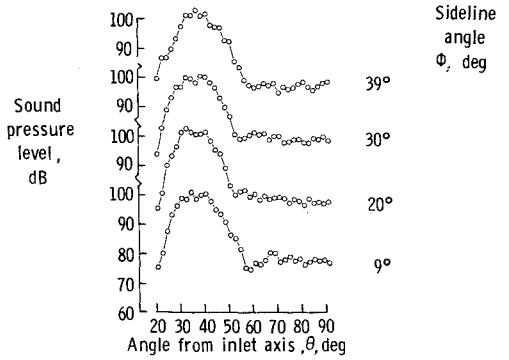


**Fig. 11 Sideline directivity patterns of BPF tone at $ka = 22.9$.**

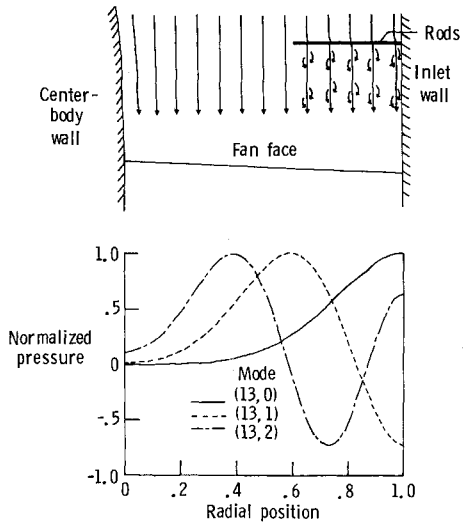


**Fig. 12 Radial dependence of normalized pressure for various modes.**

### Comparison with Static Test and Theory

BPF tone directivity patterns for static and flight tests are compared in Fig. 13 for two values of $ka$. The static data were taken directly from Ref. 7. Recall that except for the bandwidth of analysis, the static data were processed and normalized in a fashion similar to the flight data. The broader bandwidth of analysis for the static data would have the effect of raising the broadband floor 8-10 dB. Since, in general, the narrowband analysis yielded a tone level near the peak radiation angle at least 20 dB above its broadband level, the bandwidth difference should have little effect on the absolute data comparison. At worst, the static data may be slightly higher at angles well off from the peak.

Recall also that no adjustment was made to the data for convective amplification. According to theory, this effect, which is present in flight but not in the static data, would increase the level in flight in the forward quadrant. For the present test, the effect would vary from about 4 dB at $\theta = 20$ deg to 0 dB at $\theta = 90$ deg. A trend of this sort is not readily apparent in the data of Fig. 13.

Both data comparisons in Fig. 13 show excellent agreement in directivity shape with the static data being higher everywhere. In the region where the radiation peaks occur, the level difference is small. Recall that the flight tests utilized a flight inlet as described in Fig. 3, whereas the static data had an inlet lip more representative of a bellmouth as well as an inlet control device. Reference 2 demonstrates that inlet geometry effects are significant only close to cut-on, and bellmouth-type inlets tend to radiate more toward the inlet axis than flight inlets. In the same report, in-duct flow is shown not to affect the directivity over the no-flow case for

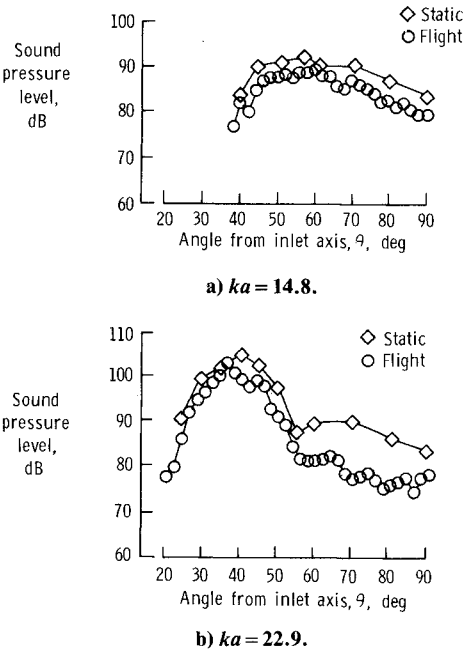


**Fig. 13 Measured BPF tone directivity comparisons; $\phi = 0$ deg.**

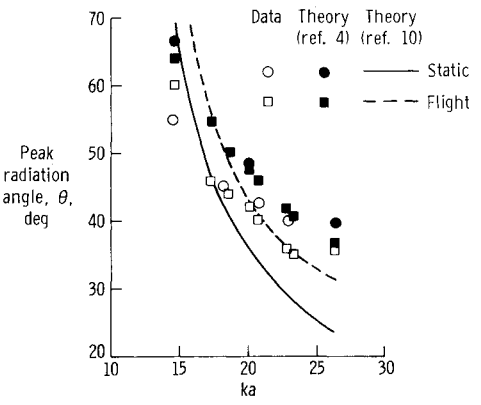


**Fig. 14 Peak radiation angle comparisons; $\phi = 0$ deg.**

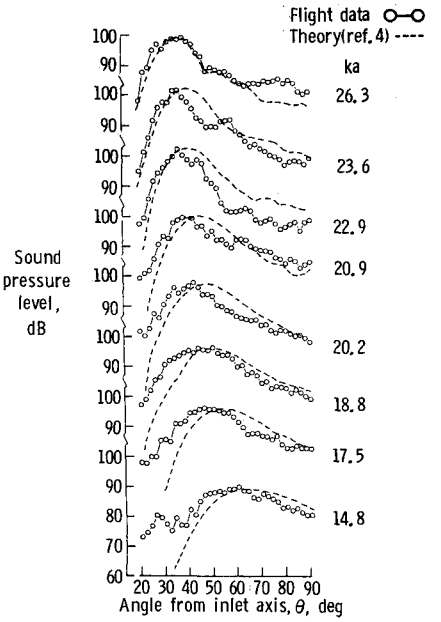


**Fig. 15 Flight BPF tone directivity comparisons; $\phi = 0$ deg.**

the same *ka*. The situation of both in-duct flow and flow over the external nacelle (which corresponds to the flight case) was not examined in Ref. 2. However, based on analytical results from Ref. 5, acoustic inlet radiation is expected to be shifted by flight to lower angles. Therefore, it is suggested that for Fig. 13a, the effect of the bellmouth geometry shifting the radiation toward the duct axis at $\xi = 1.01$ is stronger than the effect of flight shifting the radiated field toward the axis. For the higher frequency case of Fig. 13b, the geometry effect is negligible, resulting in the flight-radiated acoustic field to be shifted forward about 5 deg over the static case.

These effects are further shown by the experimental data plotted in Fig. 14, where the peak radiation angle taken from directivity plots similar to the previous figure is presented over the range of *ka* investigated. Again, the peak radiation angle is greater at lower frequencies near cut-on for the flight condition with flight inlet geometry. At *ka* values greater than 20 however, the static cases with a bellmouth geometry tend to radiate to higher angles. The peak radiation angles calculated from the theory of Ref. 4 are also presented both for the flight and static cases. Also, the approximate theory of Rice et al.[10] is shown as well. Using the theory of Ref. 4, the static cases are calculated for the same geometry (Fig. 3) as the flight cases. Therefore, no inlet geometry effect exists and the static predictions are seen to always radiate to slightly larger angles than the flight prediction, regardless of frequency. Ignoring geometry effects, the trends of the theory and experiment are quite similar, although offset noticeably in absolute value of the peak radiation angle. In contrast, the theory of Ref. 10 shows a much stronger trend of radiation angle with increasing *ka*. Also, flight causes a shift in the opposite direction to higher radiation angles.

The overall radiation directivities of the flight data are compared with the theory of Ref. 4 in Fig. 15. Although the trend toward narrower lobes and smaller peak radiation angles with increasing frequency is reasonably predicted, the lobes are offset 5-8 deg in all but the highest frequency case. Even the agreement at $ka = 26.3$ appears fortuitous in that the agreement is not consistently improving with *ka*.

The source of the offset between the prediction and measurement is not clear. Although the flowfield may not be modeled exactly, the sensitivity of the solution to the flow is not strong considering the small predicted or measured differences between static and flight shown in Figs. 13 and 14. The conditions of the flight tests were monitored closely and evaluations of tone directivity repeatability[6] show variations (less than 4 dB) in absolute levels but little in directivity shape. The previous discussion on the presence of contaminating modes suggests that this is not the cause of the offset inasmuch as other spinning mode orders would show up as changes in sideline directivities. Contaminating radial orders within $m = 13$ should not be present. At the lowest frequencies they are cut-off, yet the offset still exists.

## Concluding Remarks

A flight study of turbofan engine tone radiation patterns associated with a single acoustic mode was conducted and comparisons have been made with similar static test results and a radiation theory. The cut-on frequency (i.e., fan rpm) of the lowest order radial mode (13,0) occurred, as predicted by the Tyler-Sofrin theory. The single-lobed nature of overhead directivity patterns and the symmetry with respect to sideline angle demonstrated the absence of other significant circumferential and radial orders. In general, good agreement in tone radiation patterns was found between measured flight and static data. Near cut-on, the static data was shifted slightly forward, most likely because of its bellmouth inlet geometry. Well above cut-on, the flight directivity peak was slightly forward in agreement with current radiation theory. Radiation theory[4] closely predicted the shape of the flight directivity patterns and the trends of the theory and experiment were quite similar. In addition, the theory predicted a small "flight effect" in support of the experimental data. However, the theory consistently predicted higher values (between 5 and 8 deg) for peak radiation angles over a wide range of frequency. The cause of this offset is unclear.

## Appendix

The following equations are presented to define the inlet geometry shown schematically in Fig. 3.

Diffuser:

$$r = 9.95 - 0.030(x + 2.65) \qquad \text{for } -20.74 \le x \le -2.65$$

Throat:

$$r = 9.95 \qquad \text{for } -2.65 \le x \le 0$$

Internal lip:

$$r = 12.02 - 2.07\,[1.00 - (x/4.14)^2\,]^{0.5} \qquad \text{for } 0 \le x \le 4.14$$

External lip:

$$r = 12.02 + 4.12\{1.00 - [\,(x + 23.45)/27.59\,]^{3.36}\}^{0.5} \qquad \text{for } 0.08 \le x \le 4.14$$

External nacelle:

$$r = 14.67 - 0.268\,(x - 0.084) \qquad \text{for } -32.92 \le x \le 0.08$$

## References

[1] Ville, J. M. and Silcox, R. J., "Experimental Investigation of the Radiation from an Unflanged Duct and a Bellmouth Including the Effect of Flow," NASA TP-1697, 1980.

[2] Silcox, R. J., "Experimental Investigation of Geometry and Flow Effects on Acoustic Radiation from Duct Inlets," AIAA Paper 83-0713, April 1983.

[3] Horowitz, S. J., Sigman, R. K., and Zinn, B. T., "An Iterative Finite Element Integral Technique for Predicting Sound Radiation from Turbofan Inlets in Steady Flight," AIAA Paper 82-0124, Jan. 1982.

[4] Astley, R. J. and Eversman, W., "Wave Envelope and Infinite Element Schemes for Fan Noise Radiation from Turbofan Inlets," AIAA Paper 83-0709, April 1983.

[5] Baumeister, K. J. and Horowitz, S. J., "Finite Element-Integral Simulation of Static and Flight Fan Noise Radiation from the JT15D Turbofan Engine," NASA TM-82936, 1982.

[6] Preisser, J. S. and Chestnutt, D., "Flight Effects on Fan Noise with Static and Wind Tunnel Comparisons," AIAA Paper 83-0678, April 1983.

[7] Heidmann, M. F., Saule, A. V., and McArdle, J. G., "Analysis of Radiation Patterns of Interaction Tones Generated by Inlet Rods in the JT15D Engine," AIAA Paper 79-0581, March 1979.

[8] Golub, R. A. and Preisser, J. S., "Deveopment and Test Engine/Inlet Performance of a Vehicle for Flight Effects on Fan Noise Research," NASA TP-2254, 1984.

[9] Tyler, J. M. and Sofrin, T. G., "Axial Flow Compressor Noise Studies," *SAE Transactions*, Vol. 70, 1962, pp. 309-332.

[10] Rice, E. J., Heidmann, M. F., and Sofrin, T. G., "Modal Propagation Angles in a Cylindrical Duct with Flow and Their Relation to Sound Radiation," AIAA Paper 79-0183, Jan. 1979.